

Figure 2. 125.8-MHz ^{13}C NMR spectra of $[1-^{13}\text{C}, ^{18}\text{O}]$ acetate (20 mM): (A) prepared from $[5-^{13}\text{C}, ^{18}\text{O}]$ -(3S)-citrate by the action of citrate lyase, (B) with added $[1-^{13}\text{C}]$ acetate.

a 50% probability of containing ^{18}O at the thioester carbonyl.⁹ Since a mixed anhydride intermediate or four-center reaction is the most plausible hypothesis for acetyl-exchange, the simple binary statistics of ^{18}O occurrence in the thioester and of ^{18}O attack by the incoming carboxylate will result in a randomization of ^{18}O throughout the acetate oxygen pool—oxygen scrambling. The additional incorporation of ^{13}C into the carboxylate permits the direct measurement of ^{18}O distribution by virtue of the additive upfield shift on the ^{13}C NMR signal.³

$[5-^{13}\text{C}, ^{18}\text{O}]$ -(3S)-citrate¹⁰ was prepared by the action of citrate (*si*)-synthase [citrate oxaloacetate-lyase (CoA acetylating); EC 4.1.3.7] (Sigma) on $[1-^{13}\text{C}]$ acetyl-CoA and oxaloacetate (both generated in situ) in H_2^{18}O .¹¹ This enzyme catalyzes the hydrolysis of the initially formed citryl-CoA to incorporate the ^{18}O label from solvent. The 125-MHz ^{13}C NMR spectrum (Figure 1A) of the purified citrate reveals two resonances (85:15 relative intensity). Addition of $[5-^{13}\text{C}]$ -(3S)-citrate to the sample (Figure 1B) establishes that the minor peak in Figure 1A is due to citrate lacking the ^{18}O label. The upfield shift of the major peak (0.027 ppm) is consistent with a singly ^{18}O -labeled carboxylate.¹²

Processing of the doubly labeled citrate by citrate lyase¹³ afforded $[1-^{13}\text{C}]$ acetate whose ^{13}C NMR spectrum revealed a triplet

(9) This assumes that there is no observable isotope effect against ^{18}O attack. In reality, even a full isotope effect will have only a small effect on the statistics.

(10) The numbering system used here is that of Glusker and Srere. The *pro-R* arm is given priority (Glusker, J. P.; Srere, P. A. *Bioorg. Chem.* **1973**, *2*, 301).

(11) A typical reaction contained (in 3.0 mL 99% H_2^{18}O) 0.25 M triethanolamine, pH 8.0, 16 mM $[1-^{13}\text{C}]$ sodium acetate, 2 mM CoA, 30 mM ATP, 40 mM MgCl_2 , 20 mM L-malic acid, 30 mM NAD, 4 units of (S)-acetyl-CoA synthetase, 20 units of malate dehydrogenase, and 8 units of citrate (*si*)-synthase. The reaction, monitored by NADH production, was allowed to proceed (37 °C) to 80–90% conversion. H_2^{18}O was recovered by bulb-to-bulb distillation, and the citrate was purified by DEAE Sephadex chromatography.

(12) Risley, J. M.; Van Etten, R. L. *J. Am. Chem. Soc.* **1981**, *103*, 4389.

(13) The reaction mixture (1.0 mL with 20% $^2\text{H}_2\text{O}$ for NMR locking) contained 0.4 M triethanolamine, pH 7.6, 20 mM ZnCl_2 , 20 mM labeled citrate, 25 mM NADH, 50 units of malate dehydrogenase, 40 units of L-lactate dehydrogenase, and 10 units of citrate lyase. NADH, malate dehydrogenase, and lactate dehydrogenase are added to drive the reaction toward acetate by trapping oxaloacetate and pyruvate (formed by spontaneous decarboxylation of the former). After 10 min the mixture is heated to 100 °C for 3 min, centrifuged, filtered, and subjected to NMR analysis.

(33:49:18 relative intensity; Figure 2A). Addition of authentic $[1-^{13}\text{C}]$ acetate (Figure 2B) and the chemical shift difference between peaks (0.027 ppm) establish that the resonances are due to acetates containing 0, 1, and 2 ^{18}O 's. On the basis of the ^{18}O content of the citrate, the relative intensities of the acetate resonances constitute a statistical scrambling of the label without any observable washout.

These results directly verify an acyl-exchange process for citrate lyase and establish ^{13}C NMR as the method of choice for the analysis. While mass spectral techniques are feasible, the simplicity of execution and interpretation of the NMR analysis should be readily apparent. In addition, the method permits a distinction among possible mechanisms. For instance, a noncovalent mechanism would yield no scrambling and no washout and de novo thioester formation would result in washout of label but no scrambling. Furthermore, the method should be of use with enzymes where the evidence for acyl exchange is less secure. Experiments along these lines are in progress.

Acknowledgment. We thank the National Institutes of Health (GM 29204) for support of this research. The Brüker WM 500 NMR spectrometer is supported in part by a grant from the National Science Foundation (CHE-791620). We express our gratitude to Peter Demou and Brigitte Segmuller for expert technical assistance.

Contribution of Tunneling to Secondary Isotope Effects in Proton-Transfer Reactions¹

William H. Saunders, Jr.

Department of Chemistry, University of Rochester
Rochester, New York 14627

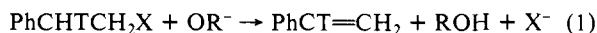
Received November 7, 1983

Calculations show that tunneling can substantially increase the magnitude of secondary hydrogen isotope effects, alter the dependence of the effects on the extent of progress along the reaction coordinate, and cause the effects to show a much steeper temperature dependence than in the absence of tunneling.

Huskey and Schowen² recently reported calculations showing that tunneling in hydride-transfer reactions can cause kinetic secondary deuterium isotope effects to exceed the corresponding equilibrium effects, thereby explaining experimental observations to this effect.^{3,4} We have found analogous anomalies with secondary tritium isotope effects in E2 reactions.

Although equilibrium isotope effects cannot be measured for E2 reactions, they can be reliably estimated from the fractionation factors of Hartshorn and Shiner.⁵ From their data, the equilibrium secondary isotope effect for complete conversion of a C—CHD—C to a C=CD—C moiety at 25 °C is 1.124. Assuming exponential temperature dependence, $(K_{\text{H}}/K_{\text{D}})_{\text{sec}}$ becomes 1.115 at 45 °C, corresponding to $(K_{\text{H}}/K_{\text{T}})_{\text{sec}} = 1.170$ (employing the usual relation between tritium and deuterium isotope effects⁶).

We have, however, observed kinetic isotope effects for reaction 1 substantially larger than the above values. When $\text{X}=\text{NMe}_3^+$



and $\text{RO}^- = \text{EtO}^-$, $(k_{\text{H}}/k_{\text{T}})_{\text{sec}}$ at 40 °C is 1.31 (corresponding to $(k_{\text{H}}/k_{\text{D}})_{\text{sec}} = 1.216$), and we have since found additional examples

(1) This work was supported by the National Science Foundation.

(2) Huskey, W. P.; Schowen, R. L. *J. Am. Chem. Soc.* **1983**, *105*, 5704–5706.

(3) Kurz, L. C.; Frieden, C. *J. Am. Chem. Soc.* **1980**, *102*, 4198–4203.

(4) Cook, P. F.; Oppenheimer, N. J.; Cleland, W. W. *Biochemistry* **1981**, *20*, 1817–1825. Cook, P. F.; Blanchard, J. S.; Cleland, W. W. *Ibid.* **1980**, *19*, 4853–4858. Cook, P. F.; Cleland, W. W. *Ibid.* **1981**, *20*, 1797–1805, 1905–1816.

(5) Buddenbaum, W. E.; Shiner, V. J., Jr. In "Isotope Effects on Enzyme-Catalyzed Reactions"; Cleland, W. W., O'Leary, M. H., Northrop, D. B., Eds.; University Park Press: Baltimore, 1977; p 11. Hartshorn, S. R.; Shiner, V. J., Jr. *J. Am. Chem. Soc.* **1972**, *94*, 9002–9012.

(6) Swain, C. G.; Stivers, E. C.; Reuwer, J. F., Jr.; Schaad, L. J. *J. Am. Chem. Soc.* **1958**, *80*, 5885–5893.

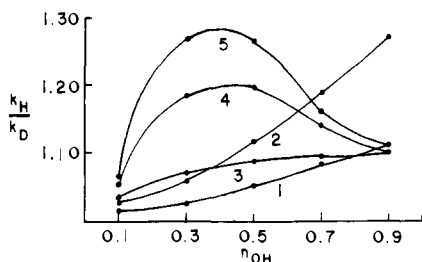


Figure 1. Plot of $(k_H/k_D)_{\text{sec}}$ vs. extent of bond formation (n_{OH}) for the reaction $\text{CCHDCH}_2\text{Cl} + \text{OH}^- \rightarrow \text{CCD}=\text{CH}_2 + \text{H}_2\text{O} + \text{Cl}^-$ at 45 °C. Models 1 and 2 include no coupling of C-D bending motions with the C--H stretch. Models 3-5 include increasing extents of such coupling. See text for details.

where $(k_H/k_T)_{\text{sec}} > (K_H/K_T)_{\text{sec}}$.^{7,8}

To explore the possibility of modeling the experimental results, kinetic isotope effect calculations were performed on reaction 2.



The model is closely similar to those used in earlier calculations,⁹ except that the geometry at the α - and β -carbons varies from tetrahedral to trigonal as the HO--H bond order (n_{OH}) varies from 0 to 1. The first set of calculations, (1) and (2), coupled only the O--H, H--C, the H--C, C--C, and the C--C, C--Cl stretches by means of off-diagonal F matrix elements, defined as

$$F_{ij} = K(F_{ii}F_{jj})^{1/2} \quad (3)$$

where K is a constant. If $K = A$ for the O--H, C--H coupling and $K = B$ for the C--H, C--C and C--C, C--X couplings, then the previously derived^{9,10} relationship becomes

$$1 - 2B^2 - A^2 + A^2B^2 = D \quad (4)$$

The curvature parameter, D , controls the magnitude of the imaginary reaction coordinate frequency. The values of A , B , and D were 1.05, 0.33, and -0.20 , respectively, as before.⁹ If the H--C stretch is also coupled with C--C-D, C--C-D, and H--C-D bends with $K = C$ in eq. 3, a new relationship between the constants can be derived as before^{9,10} and is

$$1 - A^2 - 2B^2 - C^2 + A^2B^2 - B^2C^2 = D \quad (5)$$

To ensure that $F_{\text{st},\text{bd}} \rightarrow 0$ for a reactant-like transition state (it must for a product-like one because $F_{\text{C-H}} \rightarrow 0$), C was defined as $C'n_{\text{OH}}^{1/2}$. Then A and D were assigned constant values while B and C varied with n_{OH} . For models 3-5, the sets of constants used were respectively A , 1.00, 1.00, 1.00, $|C|$,¹¹ 0.28, 0.49, 0.57, and D , -0.20 , -0.30 , -0.35 . The models thus represent increasingly strong stretch-bend coupling, and increasing barrier curvature. The tunnel corrections were calculated from the $[\nu_L^*]$ values using the first term of the Bell equation.¹²

The calculated $(k_H/k_D)_{\text{sec}}$ values at 45 °C as a function of n_{OH} (other reacting bond-order changes concerted with n_{OH}) are shown in Figure 1 for various models. Model 1, in which the bending force constants involving breaking bonds approach a constant value (simulating the sp^3 to sp^2 change) as n_{OH} approaches unity, gives a monotonic increase in k_H/k_D up to a value close to the estimated $(K_H/K_D)_{\text{sec}}$. It thus fails to account for cases in which $(k_H/k_D)_{\text{sec}}$ exceeds $(K_H/K_D)_{\text{sec}}$. Model 2, in which the bending force constants involving breaking bonds approach zero as n_{OH} approaches unity, gives much larger $(k_H/k_D)_{\text{sec}}$ values, but the limiting $(k_H/k_D)_{\text{sec}}$ as $n_{\text{OH}} \rightarrow 1.0$ is ca. 1.3, far larger than $(K_H/K_D)_{\text{sec}}$. Neither model gives an appreciable tunnel correction to $(k_H/k_D)_{\text{sec}}$.

(7) Subramanian, Rm.; Saunders, W. H., Jr. *J. Phys. Chem.* **1981**, *85*, 1099-1100.

(8) Subramanian, Rm., unpublished results from these laboratories.

(9) Saunders, W. H. *Chem. Scr.* **1975**, *8*, 27-36; **1976**, *10*, 82-89. Katz, A. M.; Saunders, W. H., Jr. *J. Am. Chem. Soc.* **1969**, *91*, 4469-4472.

(10) Melander, L.; Saunders, W. H., Jr. "Reaction Rates of Isotopic Molecules"; Wiley: New York, 1980; pp 64-66, 75-83.

(11) C' was negative for the first two bends and positive for the last.

(12) Bell, R. P. "The Tunnel Effect in Chemistry"; Chapman and Hall: New York, 1980; pp 60-63.

Table I. Temperature Dependence of $(k_H/k_D)_{\text{sec}}$ in the Reaction $\text{CCHDCH}_2\text{Cl} + \text{OH}^- \rightarrow \text{CCD}=\text{CH}_2 + \text{Cl}^- + \text{H}_2\text{O}$

model ^a	n_{OH}	$(k_H/k_D)_{\text{sec,sc}}^b$	$(k_H/k_D)_{\text{sec}}$	ΔE_a^c	A_H/A_D^c	$\nu_{\text{LH}}^*/\nu_{\text{LD}}^*$
1	0.5	1.048	1.053	0.045	0.981	1.002
	0.9	1.113	1.113	0.092	0.963	1.009
2	0.5	1.113	1.117	0.097	0.958	1.002
	0.9	1.272	1.273	0.238	0.913	1.007
3	0.3	1.032	1.069	0.082	0.938	1.019
	0.5	1.058	1.088	0.089	0.945	1.017
4	0.3	1.031	1.184	0.445	0.587	1.037
	0.5	1.056	1.197	0.374	0.663	1.039
5	0.3	1.027	1.270	0.950	0.284	1.041
	0.5	1.052	1.267	0.670	0.440	1.045

^a See text and legend to Figure 1. ^b The semiclassical (without tunneling) isotope effect at 45 °C. ^c From least-squares fits to Arrhenius equation over the range 25-55 °C.

Models 3-5, on the other hand, do give significant tunnel corrections to $(k_H/k_D)_{\text{sec}}$. Models 4 and 5 give $(k_H/k_D)_{\text{sec}} > (K_H/K_D)_{\text{sec}}$ in the range $n_{\text{OH}} = 0.3-0.7$, but in all three models $(k_H/k_D)_{\text{sec}}$ approaches $(K_H/K_D)_{\text{sec}}$ as $n_{\text{OH}} \rightarrow 1.0$. Model 4 most closely matches the experimental results.^{7,8} All of these models generate reasonable maximum values (6-9) for $(k_H/k_D)_{\text{prim}}$.

Since models 3-5 show little or no relation between $(k_H/k_D)_{\text{sec}}$ and the extent of rehybridization ($= n_{\text{OH}}$) in the transition state, what does $(k_H/k_D)_{\text{sec}}$ reflect? The $\nu_{\text{LH}}^*/\nu_{\text{LD}}^*$ values in Table I are clearly largest when $(k_H/k_D)_{\text{sec}}$ is largest. Thus $(k_H/k_D)_{\text{sec}}$ reflects the extent to which motion of the nontransferred β -hydrogen contributes to the motion along the reaction coordinate.

An experimental criterion for tunneling other than $(k_H/k_D)_{\text{sec}} > (K_H/K_D)_{\text{sec}}$ is afforded by the temperature dependence of $(k_H/k_D)_{\text{sec}}$. Although $A_H/A_D > 0.9$ for models 1 and 2, models 3-5 can generate much smaller A_H/A_D values—around 0.6-0.7 for $(k_H/k_D)_{\text{sec}} = 1.20$ and as low as 0.3 for $(k_H/k_D)_{\text{sec}} = 1.27$ (Table I). These anomalous Arrhenius parameters should be easy to demonstrate experimentally, and we are currently engaged in such efforts with $(k_H/k_T)_{\text{sec}}$ measurements. The isotope effects in the figure and table, incidentally, can be converted to $(k_H/k_T)_{\text{sec}}$ by the usual relationship.⁶ Agreement with separately calculated $(k_H/k_T)_{\text{sec}}$ values is not exact but reasonably close.

Novel Tricosahedral Structure of the Largest Metal Alloy Cluster: $[(\text{Ph}_3\text{P})_{12}\text{Au}_{13}\text{Ag}_{12}\text{Cl}_6]^{m+}$

Boon K. Teo* and Kelly Keating

AT&T Bell Laboratories
Murray Hill, New Jersey 07974

Received December 13, 1983

Recently there has been considerable interest in high-nuclearity close-packed metal cluster compounds¹ with metal arrangements resembling fragments of metallic lattices and/or surfaces, particularly in relation to catalysis and surface sciences. We report here preliminary results of the structure of a novel 25-atom cluster containing 13 Au and 12 Ag atoms: $[(\text{Ph}_3\text{P})_{12}\text{Au}_{13}\text{Ag}_{12}\text{Cl}_6]^{m+}$ (1). This cationic cluster, with the unprecedented geometry of three interpenetrating icosahedra, represents the largest metal alloy (mixed-metal) cluster known to date.

The title compound was prepared by reducing a mixture (Au:Ag = 1:1) of Ph_3PAuCl and $(\text{Ph}_3\text{P})_4\text{Ag}_4\text{Cl}_4$ with NaBH_4 in ethanol. Synthetic and spectroscopic details will be published separately. The molecular architecture of the cation, as obtained from eth-

(1) For reviews, see: (a) Chini, P. *Gazz. Chim. Ital.* **1979**, *109*, 225; (b) *J. Organomet. Chem.* **1980**, *200*, 37; (c) Chini, P., Longoni, G., Albano, V. G. *Adv. Organomet. Chem.* **1976**, *14*, 285; (d) "Transition Metal Clusters"; Johnson, B. F. G., Ed.; Wiley-Interscience: Chichester, 1980.

(2) Teo, B. K.; Calabrese, J. C. *Inorg. Chem.* **1976**, *15*, 2467.